Molecular and Electronic Analysis of (7-Chloro-2-oxo-2H-chromen-4-yl)-methyl diethylcarbamodithioate by DFT and HF Calculations

M. Evecen* and H. Tanak
Department of Physics, Faculty of Arts and Sciences, Amasya University, Amasya, Turkey

(Received August 28, 2015; in final form May 12, 2019)

The molecular geometry and vibrational frequencies of (7-chloro-2-oxo-2H-chromen-4-yl)-methyl diethylcarbamodithioate in the ground state have been calculated by using the Hartree–Fock and density functional theory methods (B3LYP and B3PW91) with 6-311++G(d,p) basis set. The results of the optimized molecular structure are presented and compared with the experimental X-ray data. The calculated vibrational frequencies are used to determine the types of molecular motions associated with each of the experimental bands observed. To investigate the nonlinear optics properties of the title compound, the polarizability and the first hyperpolarizability are calculated using the density functional B3LYP method. The predicted nonlinear optical properties of the title compound are greater than ones of urea. To determine conformational flexibility, molecular energy profile of the title compound is obtained by B3LYP calculations with respect to selected degree of torsional freedom, which is varied from -180° to $+180^\circ$ in steps of 10°. Besides, molecular electrostatic potential, natural bond orbitals, natural atomic charges, frontier molecular orbitals, and several thermodynamic properties are performed by the density functional theory methods.

DOI: 10.12693/APhysPolA.136.3
PACS/topics: HF, DFT, coumarins, NBO, MEP

1. Introduction

Coumarins are obtained from both natural products and synthetic methods and also their derivatives possess potential biological activity such as antimicrobial [1], antifungal [2], anti-HIV [3], antioxidant [4], anticancer [5], antiviral [6], tuberculostatic [7], antitumor [8], antivascular [9], TNF-α inhibitor [10], anticoagulant [11], estrogenic [12], anti-inflammatory [13], and anticonvulsant activity [14, 15]. Some coumarin derivatives have also been used in laser dyes, non-linear optical chromophores, photoluminescent materials, fluorescent whiteners, fluorescent probes, and solar energy collectors [16–21]. On the other hand, it is known that they are used as additives in food and cosmetics [22].

Investigations into the structural stability of these compounds using both experimental techniques and theoretical methods have been of interest for many years. With recent advances in computer hardware and software, it is possible to correctly describe the physicochemical properties of molecules from first principles using various computational techniques [23]. In recent years, density functional theory (DFT) has been the shooting star in theoretical calculations. The development of ever better exchange-correlation functionals has made it possible to calculate many molecular properties with accuracies comparable to those of traditional correlated *ab initio* methods, at more favourable computational costs [24]. Literature surveys have revealed the high degree of accuracy of DFT methods in reproducing the experimental values in terms of geometry, dipole moment, vibrational frequency, etc. [25–27].

In previous publication, the X-ray, infrared (IR), ^{1}H-NMR of (7-chloro-2-oxo-2H-chromen-4-yl)-methyl diethylcarbamodithioate were studied [28]. In spite of it being very essential, as mentioned above, there is no published theoretical calculation on (7-chloro-2-oxo-2H-chromen-4-yl)-methyl diethylcarbamodithioate yet. In the present study, the molecular structure, vibrational spectra and assignments, frontier molecular orbital energies, conformational properties, natural bond orbitals, natural atomic charges, nonlinear optical properties, and thermodynamical parameters were investigated on (7-chloro-2-oxo-2H-chromen-4-yl)-methyl diethylcarbamodithioate. The aim of this study is to investigate the spectral and structural properties of the coumarin compound, (7-chloro-2-oxo-2H-chromen-4-yl)-methyl diethylcarbamodithioate, using the Hartree–Fock (HF) and DFT (B3LYP, B3PW91) calculations and then compare our results with the available experimental work published before.

2. Computational methods

The initial molecular geometry was directly taken from the X-ray diffraction experimental result without any constraints [28]. The geometry optimization is the first step for the theoretical calculations. The geometry optimizations of the molecule were performed using the HF and DFT (B3LYP and B3PW91) methods with the 6-311++G(d,p) basis set. Theoretical calculations of the

*corresponding author; e-mail: meryem.evecen@amasya.edu.tr

title compound were performed using the Gaussian 09W program [29]. The obtained vibrational frequencies were scaled by 0.89 for HF, 0.96 for B3LYP, and 0.957 for B3PW91. The verification of the normal modes assignment was made using the Gaussview molecular visualisation program [30]. In addition, the thermodynamic properties, electronic properties, natural bond orbital (NBO), HOMO–LUMO energies were calculated using DFT/B3LYP method.

3. Results and discussion

3.1. Molecular structure

The crystal structure [28] and the theoretical geometric structure of the title compound are shown in Fig. 1a and b. The crystal structure of the title compound is monoclinic and space group is $P2_1/c$. The crystal structure parameters of the title compound are $a = 7.7005(2)$ Å, $b = 23.3452(8)$ Å, $c = 9.7016(3)$ Å, $\beta = 110.349(2)°$, and $V = 1635.21(9)$ Å^3 [28]. The molecular structure of the title crystal belongs to C_1 point group symmetry. The optimized parameters (bond lengths, bond angles, and torsion angles) of the title compound have been obtained by HF, B3LYP and B3PW91 methods with the 6-311++G(d,p) basis set. Theoretical and experimental geometric parameters are listed in Table I.

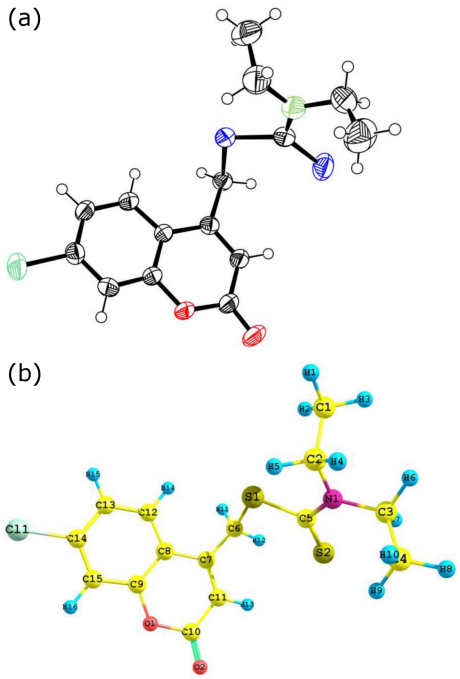

Fig. 1. (a) The experimental geometric structure of the title compound [28]. (b) The theoretical geometric structure of the title compound (with B3LYP/6-311++G(d,p) level). Visualization of this structure has been carried out with ChemCraft software [31].

Selected molecular structure parameters TABLE I

Bond lengths	Exp. [28]	HF	B3LYP	B3PW91
Cl1–C14	1.735	1.739	1.753	1.740
S1–C5	1.783	1.791	1.821	1.806
S1–C6	1.806	1.822	1.838	1.823
S2–C5	1.662	1.673	1.671	1.665
O1–C10	1.373	1.352	1.399	1.392
O1–C9	1.379	1.346	1.360	1.354
O2–C10	1.205	1.178	1.202	1.200
N1–C5	1.330	1.326	1.349	1.345
N1–C3	1.474	1.473	1.477	1.468
N1–C2	1.477	1.470	1.475	1.466
C1–C2	1.513	1.526	1.531	1.525
C3–C4	1.498	1.524	1.529	1.523
C6–C7	1.498	1.508	1.505	1.499
C7–C11	1.344	1.332	1.355	1.354
C7–C8	1.451	1.467	1.454	1.450
C8–C9	1.392	1.388	1.407	1.404
C8–C12	1.404	1.396	1.406	1.403
C9–C15	1.373	1.386	1.395	1.393
C10–C11	1.437	1.466	1.454	1.451
C12–C13	1.370	1.376	1.385	1.383
C13–C14	1.378	1.388	1.398	1.396
C14–C15	1.375	1.374	1.385	1.383
RMSE[a]		0.0156	0.0184	0.0142
max. difference[a]		0.033	0.038	0.025
Bond angles	Exp. [28]	HF	B3LYP	B3PW91
C5–S1–C6	104.12	105.72	103.36	102.93
C10–01–C9	121.54	123.26	122.37	122.40
C5–N1–C3	120.80	120.94	120.61	120.49
C5–N1–C2	123.70	124.78	124.44	124.24
C3–N1–C2	115.40	114.28	114.96	115.27
N1–C2–C1	112.40	113.26	113.42	113.39
N1–C2–H4	109.10	106.46	106.64	106.69
N1–C2–H5	109.10	109.68	108.97	108.88
N1–C3–C4	112.00	112.71	112.78	112.71
N1–C3–H6	109.20	106.51	106.71	106.76
N1–C3–H7	109.20	108.69	108.01	107.90
N1–C5–S2	124.23	124.33	124.38	124.23
N1–C5–S1	112.71	113.63	112.57	112.51
S2–C5–S1	123.04	122.02	123.04	123.24
C7–C6–S1	111.11	113.43	112.98	112.62
S1–C6–H11	109.40	104.61	105.35	105.85
S1–C6–H12	109.40	107.97	105.96	105.69
C11–C7–C8	118.60	118.79	119.04	118.97
C11–C7–C6	120.90	120.42	120.01	120.12
C8–C7–C6	120.47	120.78	120.95	120.91
C9–C8–C12	117.00	117.58	117.48	117.60
C9–C8–C7	118.45	117.42	117.72	117.69
C12–C8–C7	124.50	124.99	124.79	124.71
C15–C9–O1	115.93	116.09	116.19	116.21
C15–C9–C8	122.90	122.04	121.87	121.77
O1–C9–C8	121.17	121.87	121.94	122.03
O2–C10–O1	116.50	118.73	117.61	117.62

TABLE I (cont.)

Bond angles	Exp. [28]	HF	B3LYP	B3PW91
O2–C10–C11	126.20	124.86	126.45	126.35
O1–C10–C11	117.40	116.41	115.94	116.03
C7–C11–C10	122.80	122.24	122.98	122.88
C13–C12–C8	121.10	121.57	121.62	121.61
C12–C13–C14	119.20	118.87	118.95	118.94
C15–C14–C13	122.10	121.48	121.56	121.52
C15–C14–Cl1	118.57	119.25	119.22	119.23
C13–C14–Cl1	119.29	119.28	119.23	119.25
C9–C15–C14	117.60	118.46	118.52	118.57
RMSE[a]		1.0977	0.7483	0.7290
max. difference[a]		4.79	4.05	3.71
Torsion angles	Exp. [28]	HF	B3LYP	B3PW91
C5–N1–C2–C1	−87.50	−91.91	−92.41	−92.43
C3–N1–C2–C1	92.00	87.82	87.19	87.16
C5–N1–C3–C4	−89.00	−89.64	−89.69	−89.47
C2–N1–C3–C4	91.40	90.62	90.69	90.92
C3–N1–C5–S2	1.60	0.98	1.59	1.51
C2–N1–C5–S2	−178.90	−179.30	−178.83	−178.92
C3–N1–C5–S1	−176.80	−177.31	−176.83	−176.93
C2–N1–C5–S1	2.70	2.41	2.75	2.65
C6–S1–C5–N1	−172.85	−173.23	−173.61	−173.74
C6–S1–C5–S2	8.80	8.43	7.95	7.80
C7–C6–S1–C5	93.46	95.77	100.75	101.23
S1–C6–C7–C11	−108.00	−108.45	−105.76	−105.99
S1–C6–C7–C8	70.40	72.81	74.83	74.42
C11–C7–C8–C9	1.40	0.74	0.30	0.22
C6–C7–C8–C9	−177.00	−179.50	−179.72	−179.82
C11–C7–C8–C12	−178.60	−178.67	−179.47	−179.60
C6–C7–C8–C12	2.90	0.09	−0.06	0.00
C10–O1–C9–C15	−179.10	−178.78	−179.53	−179.64
C10–O1–C9–C8	0.80	−1.09	−0.44	−0.33
C12–C8–C9–C15	−2.10	−0.25	−0.03	0.01
C7–C8–C9–C15	177.90	179.70	179.82	179.82
C12–C8–C9–O1	178.11	179.61	179.94	179.99
C7–C8–C9–O1	−2.00	0.16	0.15	0.16
C9–O1–C10–O2	−179.30	−179.03	−179.67	−179.78
C9–O1–C10–C11	0.90	1.04	0.27	0.13
C8–C7–C11–C10	0.20	−0.78	−0.48	−0.42
C6–C7–C11–C10	178.60	179.54	179.90	179.97
O2–C10–C11–C7	178.30	179.99	178.86	179.85
O1–C10–C11–C7	−1.40	−0.08	0.20	0.26
C9–C8–C12–C13	1.70	0.16	0.07	0.05
C7–C8–C12–C13	−178.20	−179.57	−179.84	−179.87
C8–C12–C13–C14	−0.30	0.05	−0.01	−0.02
C12–C13–C14–C15	−0.80	−0.19	−0.10	−0.08
C12–C13–C14–Cl1	179.55	179.92	179.97	179.98
O1–C9–C15–C14	−179.10	−179.75	−179.96	−179.92
C8–C9–C15–C14	1.00	0.12	−0.07	−0.11
C13–C14–C15–C9	0.50	0.10	0.13	0.14
Cl1–C14–C15–C9	−179.90	−180.00	−179.93	−179.92

Note: [a]RMSE and maximum differences between the bond lengths and angles computed using theoretical methods and those obtained from X-ray diffraction.

As seen from Table I, most of the calculated bond lengths, bond angles and torsion angles are slightly different from the experimental data. Comparative graphs of the bond lengths, bond angles, and torsion angles are presented in Figs. 2–4. We noted that the experimental results belong to the solid phase and theoretical calculations belong to the gas phase. In the solid state, the existence of the crystal field along with the intermolecular interactions has connected the molecules together, which results in differences in bond parameters between the calculated and experimental values [32, 33]. The biggest differences of bond lengths between the experimental and the calculated values are obtained at S1–C5 bond, with the different values being 0.038 Å for B3LYP, O1–C9 bond with a value 0.029 Å for HF, and 0.025 Å for B3PW91 method. For the bond angles, the biggest differences occur at S1–C6–H11 with the different values being 4.761° for HF and 4.053° for B3LYP and S1–C6–H12 bond angle with the different values being 3.713° for B3PW91 method. If you look at the terms of unhydrogenated bond angles, the biggest differences occur at C7–C6–S1 with the different values being 2.318° for HF method, 1.868° for B3LYP method, and 1.511° for B3PW91 method and also O2–C10–O1 bond angle with the different values being 2.233° for HF method, 1.109° for B3LYP method, and 1.116° for B3PW91 method.

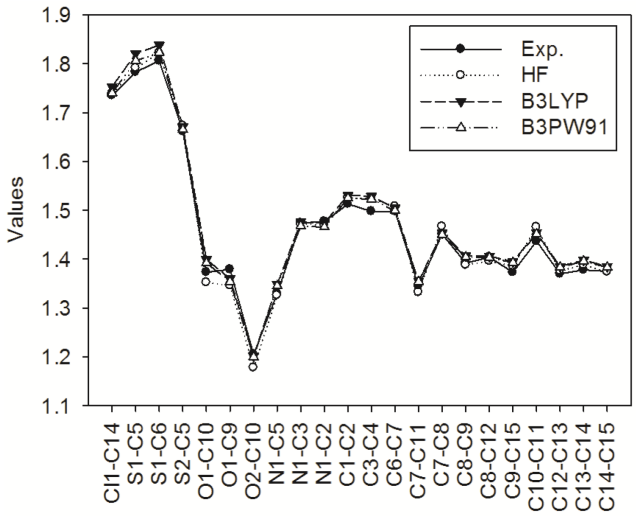

Fig. 2. Bond length differences between experimental and theoretical methods.

In order to compare the theoretical results with the experimental values, root mean square error (RMSE) is used. Calculated RMSE for bond lengths and bond angles are 0.0156 Å and 1.0977° for HF, 0.0184 Å and 0.7483° for B3LYP, and 0.0142 Å and 0.7290° for B3PW91, respectively. According to these results, it may be concluded that the B3PW91 calculation well reproduce the bond lengths and angles of the title compound. In spite of these differences, the DFT optimized geometries represent a good approximation with the crystal structure.

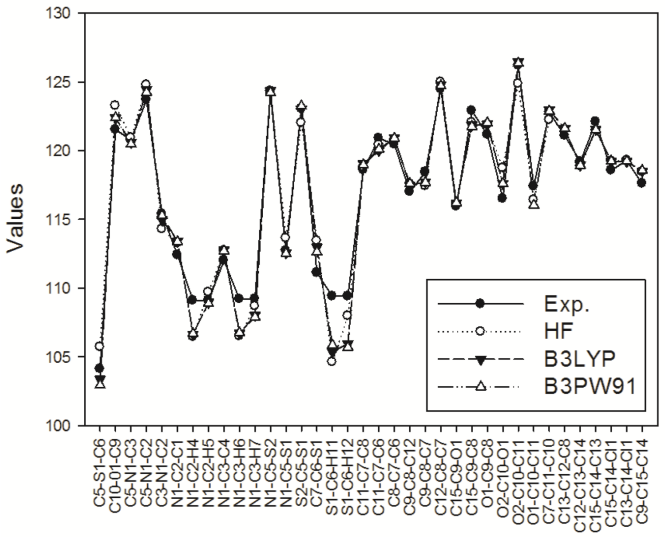

Fig. 3. Bond angle differences between experimental and theoretical methods.

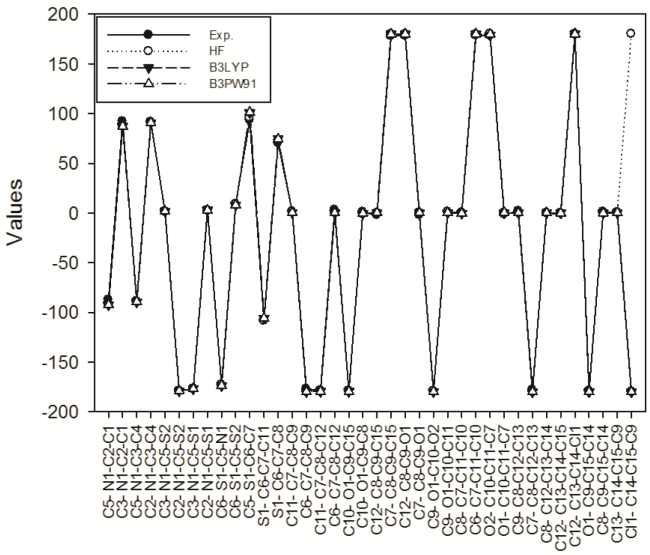

Fig. 4. Dihedral angle differences between experimental and theoretical methods.

In order to define the preferential position of the low energy structures using B3LYP/6-311++G(d,p) computations were performed as a function of the selected degrees of torsional freedom T (C7–C6–S1–C5). The respective values of the selected degrees of torsional freedom T (C7–C6–S1–C5) is 93.46° in X-ray structure [28], whereas the corresponding values in B3LYP optimized geometry is 100.75°. Molecular energy profile with respect to rotation about the selected torsion angles are given in Fig. 5. According to the results, the low energy domains for T (C7–C6–S1–C5) are located from −180° to −120° and from 60° to 180°, which is in agrement with the optimized geometry value. Energy difference between the most favorable (−140°) and unfavorable (−70°) conformers is found to be 25.67 eV when selected degree of torsional freedom is considered. It must be remarked that the conformational analysis of the title compound in the selected torsion angle was separated near to its value in the global minimum.

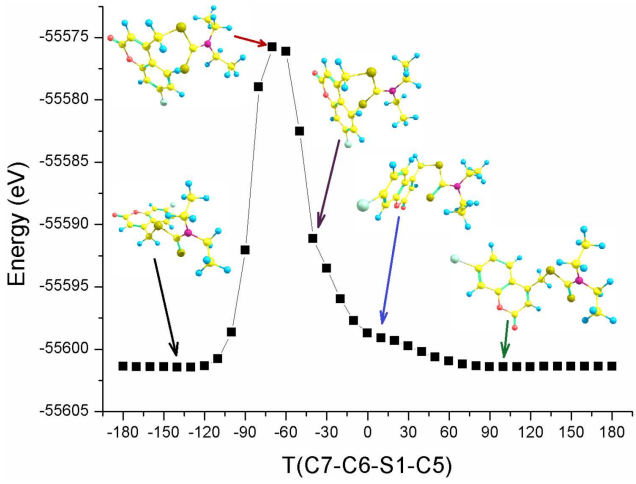

Fig. 5. Potential energy profile using B3LYP/6-311++G(d.p) method for the internal rotation around the C6-S1 bond of the title compound. Visualization of this structure has been carried out with ChemCraft software [31].

3.2. Vibrational spectra

Harmonic vibrational frequencies were calculated using the HF, DFT/B3LYP and DFT/B3PW91 methods with the 6-311++G(d,p) basis set. Simulated IR spectra of the title compound are shown in Fig. 6. Using the Gauss-View molecular visualisation program, the vibrational band assignments were made. In order to facilitate assignment of the observed peaks, we investigated the vibrational frequencies and compared with experimental results. The theoretical and experimental results were tabulated in Table II.

The title compound $C_{15}H_{16}ClNO_2S_2$ includes 37 atoms and therefore undergoes 105 normal modes of vibrations. Among the 105 normal modes of vibrations, 71 modes of vibrations are in plane and remaining 34 modes are out of plane. The bands that are in the plane of the molecule are represented as A' and out-of-plane as A''. Thus, the 105 normal modes of vibrations of the title compound are distributed as $\Gamma_{vib} = 71A' + 34A''$. Calculated vibrational frequencies are scaled as 0.890, 0.960, and 0.957 for HF, B3LYP, and B3PW91, respectively [34, 35]. The IR spectra contain some characteristic bands of the stretching vibrations of the C–H, C–H_3, C–H_2, C=O, C–O, C–C, C–N, and C–S groups, which were analysed in a detailed way in the following.

TABLE II

Comparison of the experimental and calculated vibrational frequencies (cm^{-1})

Assignments[a]	Exp. [28]	HF	B3LYP	B3PW91
ν(C–H) s		3018	3089	3089
ν(C–H) s		3008	3084	3083
ν(C–H) as		2988	3065	3061
ν(C–H_3) as + ν(C–H_2) as		2924	3001	3000
ν(C–H_3) as + ν(C–H_2) as		2879	2994	2986
ν(C–H_2) s + ν(C–H_3) as		2870	2937	2932
ν(C–H_2) s		2860	2931	2926
ν(C–H_2) s + ν(C–H_3) s		2824	2929	2914
ν(C–H_3) s		2820	2914	2913
ν(C–H_3) as + ν(C–H_2) s		–	2912	2909
ν(C=O)	1721	1777	1734	1748
ν(C=C) R as + γ(C–H) R		1594	1570	1600
ν(C=C) R s		1543	1517	1581
ν(C–N) + δ(C–H_2)		1483	1466	1460
α(C–H_2) + α(C–H_3)		1453	1447	1435
α(C–H_2)		1419	1406	1415
ν(C–N) + α(C–H_2)		1407	1395	1392
ν(C–C) R as		1382	1375	1350
ω(C–H_3)		1347	1359	1347
ν(C–C) R as + γ(C–H) R		1345	1350	–
ω(C–H_2) + ω(C–H_3)		1257	1336	1327
ν(C–C) R		1248	1296	1318
ν(C–N) + δ(C–H_2) + ω(C–H_3)		1247	1247	1246
ν(C=S) + ν(C–C)s + ω(C–H_2)	1270	1196	1226	1233
ν(C–O–C) + γ(C–H) R	1202	1126	1212	1214
γ(C–H_3) + ν(C–N)		1074	1177	1181
α(C–H) R		1061	1126	1122
γ(C–H_3) + γ(C–H_2) + ν(C–N)		1048	1120	1116
ν(C–O) R as	1087	968	1101	1115
ν(C–Cl) + γ(C–H) R		952	1054	1056
ν(C–N)		941	1037	1042
ν(C–C) + ν(C–S)		877	972	988
ν(S–C–S) + ν (C–C)s		860	940	952
δ(C–H) R		874	924	917
ν(C–O)R + δ(C–H)R + ν(C–Cl)		860	922	931
ν(C–S) + ν(C–N)	856	833	885	894
δ(C–H) R		816	819	838
ν(C–N) + ν(C–S)		798	796	801
ω(C–H) R		757	791	787
ν(S–CH_2) s + γ(C=O)		730	704	710
ν(C–Cl) + ν(C–S) s	675	616	609	613
ν(C–S) s		367	361	365

[a] ν — stretching, α — scissoring, γ — rocking, δ — twisting, ω — wagging, s — symmetric, as — asymmetric, R — ring

3.2.1. C–H vibrations

C–H has a well known characteristic vibrational frequency, the in-plane and out-of-plane bending vibrational frequencies within characteristic region. Aromatic compounds commonly exhibit multiple weak bands in the region 3100–3000 cm^{-1} [36] which is the characteristic region for the ready identification of C–H stretching vibrations in plane. In this region, the bands are not appreciably affected by the nature of the substituents. In the present work, C–H aromatic stretchings are in the expected region, lie within the range 3018–2988 cm^{-1} by HF, 3089–3065 cm^{-1} by B3LYP, and 3089–3061 cm^{-1} by B3PW91. Besides, C–H in-plane and out-of-plane bending vibrations lied in the range 1500–1100 cm^{-1} and 1000–750 cm^{-1} [37], respectively. In this case, four bands are assigned to C–H in-plane bending vibrations of title compound, identified at 1594, 1345, 1126, and 1061 cm^{-1} by HF, 1570, 1350, 1212, and 1126 cm^{-1} by B3LYP and 1600, 1214, and 1122 cm^{-1} by B3PW91. The three out-of-plane twisting bending modes at 874, 860, and 816 cm^{-1} by HF, 924, 922, and 819 cm^{-1} by B3LYP and 917, 931 and 838 cm^{-1} by B3PW91 and an out-of-plane wagging at 757 cm^{-1} by HF, 791 cm^{-1} by B3LYP, and 787 cm^{-1} by B3PW91 are observed.

3.2.2. Methyl group vibrations (C–H_3)

The title molecule possesses two C–H_3 group. The C–H methyl group stretching vibrations are highly localized and generally observed in the range 3000–2900 cm^{-1} [38, 39]. In this study, the asymmetric bands with high peaks are found at 2924, 2879, and 2870 cm^{-1} by HF, 3001, 2994, 2937, and 2912 cm^{-1} by B3LYP and 3000, 2986, 2932, and 2909 cm^{-1} by B3PW91, while it is found at 2824 and 2820 cm^{-1} by HF, 2929 and 2914 cm^{-1} by B3LYP and 2914, and 2913 cm^{-1} by B3PW91 symmetric stretching vibrations. In this investigation, the scissoring bending mode is found at 1453 cm^{-1} by HF, 1447 cm^{-1} by B3LYP, and 1435 cm^{-1} by B3PW91, while observing two rocking frequency identified at 1074 and 1048 cm^{-1} by HF, 1177, and 1120 cm^{-1} by B3LYP and 1181 and 1116 cm^{-1} by B3PW91. C–H_3 three wagging vibrations are also found at 1347, 1257, and 1247 cm^{-1} by HF and 1359, 1336, and 1247 cm^{-1} by B3LYP and 1347, 1327, and 1246 cm^{-1} by B3PW91. This assignment is authenticated by the literature [40, 41].

3.2.3. Methylene vibrations (C–H_2)

In our present work, six stretching, three scissoring, and one rocking out-of-plane deformation vibrations, two wagging and two twisting in plane methylene vibration are found. In literature, the symmetric C–H_2 stretching vibrations are generally observed between 3000 and 2900 cm^{-1} [42]. In agreement with this, C–H_2 asymmetric modes are observed sharply at 2924 and 2879 cm^{-1} by HF, 3001 and 2937 cm^{-1} by B3LYP, and 3000 and 2932 cm^{-1} by B3PW91 while symmetric modes are found at 2870, 2860, and 2824 cm^{-1} by HF, 2937, 2931, and 2929 cm^{-1} by B3LYP and 2932, 2926, and 2914 cm^{-1} observed by B3PW91. An extra symmetric vibration is observed at 2909 cm^{-1} only by B3PW91. The C–H_2 three scissoring in plane deformation vibrations are at 1453, 1419, and 1407 cm^{-1} by HF, at 1447, 1406, and 1395 cm^{-1} by B3LYP and at 1435, 1415, and 1392 cm^{-1} by B3PW91. A rocking vibration is found at 1048 cm^{-1},

1120 cm^{-1}, and 1116 cm^{-1} band by HF, B3LYP and B3PW91, respectively. The two C–H_2 wagging vibrations are at 1257 and 1196 cm^{-1} by HF, at 1336 and 1226 cm^{-1} by B3LYP, and at 1327 and 1233 cm^{-1} by B3PW91. Lastly two twisting vibrations are at 1483 and 1247 cm^{-1} by HF, at 1466 and 1247 cm^{-1} by B3LYP, and at 1460 and 1246 cm^{-1} by B3PW91.

3.2.4. C=O, C–O vibrations

$C = O$ and $C - -O$ vibrations are more effective to investigate the various factors in ring aromatic compounds. Frequencies of the C=O stretching absorption has a greater degree than intermolecular H bonding because of the different electro-negativities of C and O [43]. The C=O vibration appears in the expected range and shows that it is not affected much by other vibrations. The characteristic infrared absorption frequency of C=O in carbonyl group are normally strong in intensity and found in the region 1800–1690 cm^{-1} [44]. In the present study, C=O stretching vibration is identified at 1777 cm^{-1} for HF, 1734 cm^{-1} for B3LYP, and 1748 cm^{-1} for B3PW91 as a strong band. These results are in agreement with experimental value of 1721 cm^{-1}. C–O stretching band of the aromatic ring in IR spectrum is characterized by the frequencies around 1270–1230 cm^{-1} [45]. For aromatic rings, the C–O vibrations are observed at 1126 (1212, 1214), 968 (1101, 1115), and 860 (922, 931) cm^{-1} by HF (B3LYP, B3PW91) methods. These assignments were also supported by the experimental values of 1202 and 1087 cm^{11} [28].

3.2.5. C–N vibrations

Silverstein et al. [44] identified the C–N stretching absorption in the region 1382–1266 cm^{-1} for aromatic amines. Tecklenburg et al. [46] have located the C–N symmetric stretch in the region 1120–1150 cm^{-1}. The C–N stretchings are also found to be present at 1248 and 1199 cm^{-1} by Pająk et al. [47]. In the present study, all C–N stretching vibration are observed sharply at 1483, 1407, 1248, 1074, 941, 833, and 798 cm^{-1} (1466, 1395, 1247, 1177, 1037, 885, and 796 cm^{-1}; 1460, 1392, 1246, 1181, 1042, 894, and 801 cm^{-1}) by HF (B3LYP; B3PW91) methods. As seen in Table II, C–N stretching vibrations are in agreement with experimental value.

3.2.6. C=C and C–C vibrations

The aromatic stretching vibrations are very prominent, as the involved double C=C bond is in conjugation with the ring. In literature, the ring C=C and C-C stretching vibrations are expected in the region 1620–1390 cm^{-1} [48] and 1625–1280 cm^{-1} [49]. In the present work, the frequencies observed at 1594, (1570, 1600), and 1543 cm^{-1} (1517, 1581 cm^{-1}) have been assigned to C=C stretching vibrations by HF (B3LYP;B3PW91) methods and the values are almost in the expected region. The C-C stretching vibrations of title compound are observed with very strong intensity at 1382, 1345, 1248, 1196, 877, and 860 cm^{-1} (1375, 1350, 1296, 1226, 1037, and 940 cm^{-1}; 1350, 1318, 1233, 988, and 952 cm^{-1}) by HF (B3LYP;B3PW91) method.

3.2.7. C=S and C–S vibrations

The absorption bands of C=S group is obtained by Silverstein et al. in the region 1563–700 cm^{-1} [50] and the absorption bands of C–S group in the range 670–930 cm^{-1} by Colthup et al. [51, 52] with a moderate intensity. The experimental C=S vibration mode were observed to be 1270 cm^{-1} while C–S vibration modes are at 856 and 675 cm^{-1} [28]. In this study, C=S vibration mode has been calculated at 1196 cm^{-1} by HF, 1226 cm^{-1} by B3LYP, and 1233 cm^{-1} by B3PW91. The C–S stretching mode are calculated at 877, 860, 833, 616, and 367 cm^{-1} (with HF), and 972, 940, 885, 609, and 361 cm^{-1} by B3LYP and 988, 952, 894, 613, and 365 cm^{-1} by B3PW91. These vibrations coincide satisfactorily with the literature and also experimental values (see Table II).

FTIR spectrum of the title compound is obtained by HF, B3LYP and B3PW91 methods, and shown in Fig. 6. It can be concluded from Fig. 6 and Table II that except for HF method, other methods agree with each other and experiment, which comes from the fact that HF is not a correlated method. It is seen from Table II that calculated vibrational frequencies of the title compund agree well with the available experimental literature and we conclude that other presented vibrational frequencies in this work can be a reference for experimentalists.

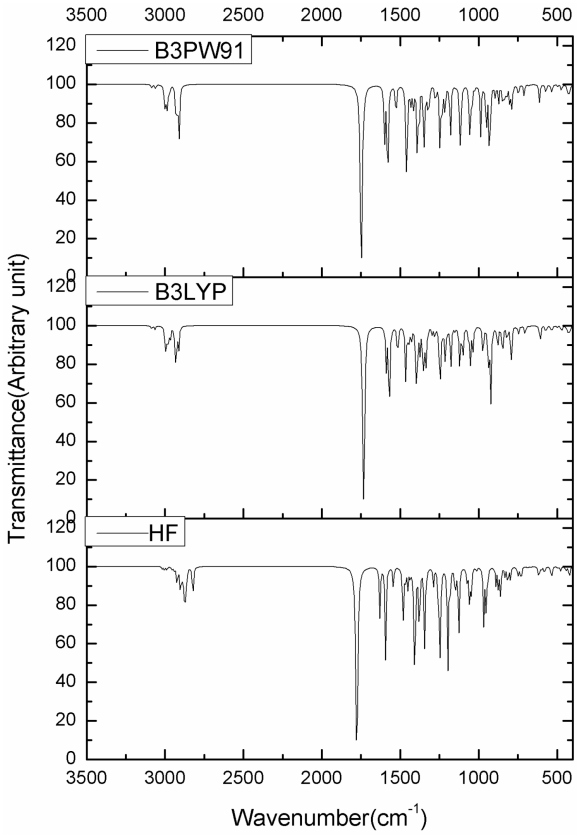

Fig. 6. Theoretical FTIR spectrum of the title compound.

3.3. Natural bond orbital analysis

We have executed NBO analysis for investigating charge transfer or conjugative interaction in molecular systems. NBO analysis was made using a program available in Gaussian 09W. Some electron donor orbital, acceptor orbital, and the interacting stabilization energy resulting from the second-order micro-disturbance theory are tabulated [53, 54]. The larger the mean of $E^{(2)}$ value is, the more intensive is the interaction between electron donors and electron acceptors [55]. The stabilization energy $E^{(2)}$ associated with i (donor) $\rightarrow$ j (acceptor) delocalization is given by the following equation [56, 57]:

$$E^{(2)} = -q_i \frac{(F_{ij})^2}{\varepsilon_j - \varepsilon_i}, \tag{1}$$

where q_i is the donor orbital occupancy, $\varepsilon_i, \varepsilon_j$ are diagonal elements (orbital energies), and F_{ij} is the off-diagonal NBO Fock matrix element. In order to investigate the intramolecular interaction, the stabilization energies of the title compound were performed using the second-order perturbation theory. The results of second-order perturbation theory analysis of the Fock matrix at B3LYP/6-311++G(d,p) level of theory are collected in Table III. For Table III, the stabilization energies larger than 3 kcal/mol have been chosen [58].

The NBO analysis has revealed that the intramolecular interactions which are formed by the orbital overlap between bonding (C–S), (C–N), (C–C), and (C–H) and anti-bonding (C–Cl), (C–S), (C–O), (C–N), (C–C), and (C–H) orbital which results in intramolecular charge transfer causing stabilization of the compound. These interactions are observed as an increase in electron density (ED) in (C–S), (C–C), (C–H), and (C–O) anti-bonding orbital that weakens the respective bonds. The electron density of dietilamina fragment (∼1.98e) clearly demonstrates strong delocalization. Similarly, the ED of conjugated bond of 2H-chromene ring (∼1.98e) clearly shows strong delocalization inside the compound [58]. Also, the hyperconjugative interactions of the $\sigma \rightarrow \sigma^*$ and $\sigma \rightarrow \pi^*$ transitions occur from various bonds in the compound. For example, the hyperconjugative interaction of the σ(C9–C15) distribute to σ^*(C14–C15) and σ^*(C15–H16) show stabilization energy of 38.23 and 9.04 kcal/mol. For chromen, in the case of σ(C14–C15) orbital the σ^*(C9–C15) and π^*(C14–C15) shows stabilization energy of 18.05 and 23.70 kcal/mol. Also σ(C15–H16) orbital the σ^*(C8–C12), σ^*(C9–C15), σ^*(C14–C15) and σ^*(C15–H16) show stabilization energy of 20.73, 26.30, 54.71, and 34.55 kcal/mol, respectively. The other hyperconjugative interaction of the σ(C15–H16) enhanced further conjugate with antibonding orbital of π^* (C14–C15), which results to strong delocalization of 28.98 kcal/mol.

π bonds must consist of p atomic orbitals of C, O, and N atoms, naturally. In the studied compound, middle degrees intramolecular hyperconjugative interactions of π-electrons occur with greater energy contributions from C7-C11 $\rightarrow$ π^*(O2–C10) (22.35 kcal/mol); C8–C9 $\rightarrow$ π^*(C7–C11) (15.59 kcal/mol) + π^*(C12–C13) (20.19 kcal/mol) and C14-C15 $\rightarrow$ π^*(C8–C9) (17.92 kcal/mol) + π^*(C4–H10) (16.53 kcal/mol). In addition, the π^*(O2–C10), π^*(C7–C11) and π^*(C12–C13) NBO conjugates with respective bonds of π^*(C7–C11), π^*(C8–C9) and σ^*(C12–C13), resulting to a stabilization of 100.07, 49.00, and 97.80 kcal/mol, respectively. The π^*(C8-C9) bond weakly interacts with σ^* (C14-C15) with the energy 10.25 kcal/mol while π^*(C14-C15) bond strongly interacts with σ^* (C14-C15) with the energy 141.19 kcal/mol. This enhanced further conjugation with antibonding orbital from π^*(C14-C15) $\rightarrow$ σ^*(C15-H16), which results to strong delocalization of 407.02 kcal/mol.

The stronger intramolecular interactions of π^*-electrons occur with the greater energy contributions from C14–C15 $\rightarrow$ σ^*(C15–H16) (407.02 kcal/mol) and σ^*(C14–C15) (141.19 kcal/mol). The interaction energy related to the resonance in the present molecule involves electron density transfer from lone pair of S2 to anti-bonding LP*(1)(C5) atom to the enormous stabilization (up to 510.28 kcal/mol). It is found that the weaker lone pairs of N1 go to anti-bonding LP*(1)(C5) atom (185.64 kcal/mol). In addition, the weaker lone pairs S1, O2, and O1 donate its electrons to the LP(1), σ, and π-type antibonding orbital.

3.4. Atomic charge analysis

In order to investigate the electron population of each atom of the title compound, the Mulliken atomic charges of the compound were calculated using the DFT/B3LYP method with the 6-311++G (d,p) basis set [59]. To investigate the solvent effect for the atomic charge distributions of title compound, based on the B3LYP/6-311++G(d,p) model and PCM method, five solvents (chloroform, ethanol, methanol, DMSO, and water) were selected and the calculated values are shown in Table IV. The Mulliken atomic charges plots are shown in Fig. 7.

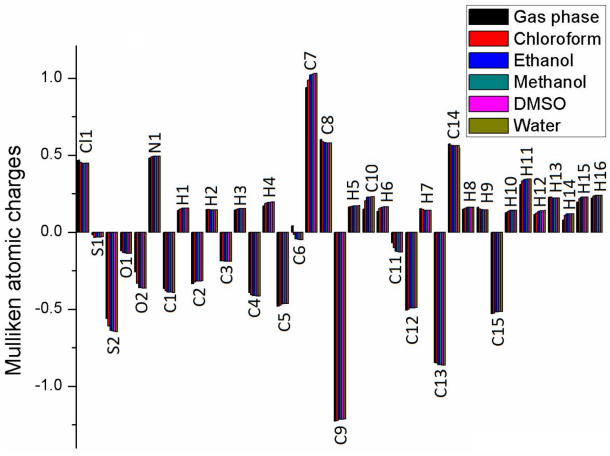

Fig. 7. Mulliken atomic charges of the title compound.

TABLE III
Selected second-order perturbation energies $E^{(2)}$ associated with $i \rightarrow j$ delocalization in gas phase

Donor orbital (i)	Type	ED/e	Acceptor orbital (j)	Type	ED/e	$E^{(2)}$ [kcal/mol][a]	$E(j)-E(i)$ [a.u.][b]	$F(i,j)$ [a.u.][c]
S1–C5	σ	1.97504	N1–C9	$\sigma*$	0.03588	5.32	0.96	0.064
S1–C6	σ	1.96681	C7–C11	$\pi*$	0.15842	3.86	0.63	0.046
S2–C5	σ	1.98253	N1–C2	$\sigma*$	0.03816	4.74	1.04	0.063
O2–C10	π	1.97860	C7–C11	$\pi*$	0.15842	5.42	0.41	0.044
N1–C2	σ	1.98252	S2–C5	$\sigma*$	0.02215	3.69	1.03	0.055
N1–C3	σ	1.97936	S1–C5	$\sigma*$	0.11755	3.81	0.87	0.053
C1–H2	σ	1.98361	N1–C2	$\sigma*$	0.03816	4.27	0.82	0.053
C2–H4	σ	1.97972	N1–C5	$\sigma*$	0.06467	3.79	0.98	0.055
C3–H6	σ	1.98027	N1–C5	$\sigma*$	0.06467	3.96	0.97	0.056
C4–H8	σ	1.98318	N1–C3	$\sigma*$	0.03588	4.12	0.81	0.052
C6–H12	σ	1.97947	C7–C8	$\sigma*$	0.03387	4.25	1.07	0.060
C7–C11	σ	1.97650	C7–C8	$\sigma*$	0.03387	3.51	1.29	0.060
C7–C11	σ	1.97650	C8–C12	$\sigma*$	0.02242	3.08	1.62	0.063
C7–C11	π	1.80323	S1–C6	$\sigma*$	0.02682	4.71	0.42	0.042
C7–C11	π	1.80323	O2–C10	$\pi*$	0.27517	22.35	0.30	0.074
C7–C11	π	1.80323	C8–C9	$\pi*$	0.42909	7.99	0.36	0.051
C8–C9	σ	1.97114	C6–C7	$\sigma*$	0.02868	3.12	1.11	0.053
C8–C9	σ	1.97114	C8–C12	$\sigma*$	0.02242	3.89	1.59	0.070
C8–C9	σ	1.97114	C9–C15	$\sigma*$	0.02222	4.73	1.50	0.075
C8–C9	π	1.59279	C7–C11	$\pi*$	0.15842	15.59	0.30	0.066
C8–C9	π	1.59279	C12–C13	$\pi*$	0.30508	20.19	0.30	0.071
C8–C12	σ	1.96930	O1–C9	$\sigma*$	0.03147	3.77	1.05	0.056
C8–C12	σ	1.96930	C7–C8	$\sigma*$	0.03387	3.92	1.25	0.063
C8–C12	σ	1.96930	C8–C9	$\sigma*$	0.03488	3.61	1.24	0.060
C8–C12	σ	1.96930	C12–C13	$\sigma*$	0.01535	3.38	1.27	0.059
C9–C15	σ	1.96576	Cl1–C14	$\sigma*$	0.03113	4.54	0.86	0.056
C9–C15	σ	1.96576	O1–C10	$\sigma*$	0.12872	4.80	1.03	0.064
C9–C15	σ	1.96576	C4–H10	$\sigma*$	0.00746	3.15	1.22	0.056
C9–C15	σ	1.96576	C7–C8	$\sigma*$	0.03387	6.51	1.27	0.081
C9–C15	σ	1.96576	C8–C9	$\sigma*$	0.03488	4.36	1.26	0.066
C9–C15	σ	1.96576	C8–C12	$\sigma*$	0.02242	7.47	1.60	0.098
C9–C15	σ	1.96576	C9–C15	$\sigma*$	0.02222	4.91	1.51	0.077
C9–C15	σ	1.96576	C10–C11	$\sigma*$	0.05423	4.43	1.34	0.069
C9–C15	σ	1.96576	C14–C15	$\sigma*$	0.02596	38.23	4.26	0.361
C9–C15	σ	1.96576	C15–H16	$\sigma*$	0.01243	9.04	4.09	0.173
C10–C11	σ	1.98150	C6–C7	$\sigma*$	0.02868	4.35	1.09	0.062
C10–C11	σ	1.98150	C7–C11	$\sigma*$	0.01954	3.01	1.32	0.056
C11–H13	σ	1.97363	O1–C10	$\sigma*$	0.12872	4.06	0.83	0.053
C11–H13	σ	1.97363	C7–C8	$\sigma*$	0.03387	5.01	1.07	0.065
C12–H14	σ	1.97782	C8–C9	$\sigma*$	0.03488	4.05	1.07	0.059
C12–H14	σ	1.97782	C13–C14	$\sigma*$	0.02840	3.41	1.08	0.054
C12–C13	σ	1.96814	Cl1–C14	$\sigma*$	0.03113	4.95	0.86	0.058
C12–C13	σ	1.96814	C7–C8	$\sigma*$	0.03387	3.42	1.26	0.059
C12–C13	σ	1.96814	C13–C14	$\sigma*$	0.02840	3.55	1.26	0.060
C12–C13	π	1.70063	C8–C9	$\pi*$	0.42909	13.79	0.34	0.063
C13–H15	σ	1.97842	C8–C12	$\sigma*$	0.02242	3.27	1.41	0.061
C14–C15	σ	1.97616	O1–C9	$\sigma*$	0.03147	5.14	1.09	0.067
C14–C15	σ	1.97616	C8–C12	$\sigma*$	0.02242	6.83	1.62	0.094
C14–C15	σ	1.97616	C9–C15	$\sigma*$	0.02222	18.05	1.53	0.148
C14–C15	σ	1.97616	C10–C11	$\sigma*$	0.05423	3.00	1.36	0.057
C14–C15	σ	1.97616	C13–H15	$\sigma*$	0.01329	4.85	1.19	0.068
C14–C15	σ	1.97616	C13–C14	$\sigma*$	0.02840	4.10	1.29	0.065

TABLE III (cont.)

Donor orbital (i)	Type	ED/e	Acceptor orbital (j)	Type	ED/e	$E^{(2)}$ [kcal/mol][a]	$E(j)-E(i)$ [a.u.][b]	$F(i,j)$ [a.u.][c]
C14–C15	σ	1.97616	C14–C15	$\sigma*$	0.02596	10.26	4.28	0.187
C14–C15	σ	1.97616	C14–C15	$\sigma*$	0.02596	10.26	4.28	0.187
C14–C15	σ	1.97616	C14–C15	$\pi*$	0.37626	23.70	3.44	0.281
C14–C15	σ	1.97616	C15–H16	$\sigma*$	0.01243	7.17	4.11	0.154
C14–C15	π	1.69984	C8–C9	$\pi*$	0.42909	17.92	0.35	0.074
C14–C15	π	1.69984	C12–C13	$\pi*$	0.30508	16.53	0.31	0.064
C15–H16	σ	1.97465	C4–H10	$\sigma*$	0.00746	8.20	1.02	0.082
C15–H16	σ	1.97465	C7–C8	$\sigma*$	0.03387	3.97	1.06	0.058
C15–H16	σ	1.97465	C8–C9	$\sigma*$	0.03488	4.15	1.05	0.059
C15–H16	σ	1.97465	C8–C9	$\pi*$	0.42909	8.13	0.59	0.069
C15–H16	σ	1.97465	C8–C12	$\sigma*$	0.02242	20.73	1.39	0.152
C15–H16	σ	1.97465	C9–C15	$\sigma*$	0.02222	26.30	1.30	0.165
C15–H16	σ	1.97465	C10–C11	$\sigma*$	0.05423	12.02	1.13	0.105
C15–H16	σ	1.97465	C13–C14	$\sigma*$	0.02840	5.12	1.06	0.066
C15–H16	σ	1.97465	C14–C15	$\sigma*$	0.02596	54.71	4.06	0.421
C15–H16	σ	1.97465	C14–C15	$\pi*$	0.37626	28.98	3.22	0.300
C15–H16	σ	1.97465	C15–H16	$\sigma*$	0.01243	34.55	3.89	0.328
Cl1	LP(2)	1.97119	C13–C14	$\sigma*$	0.02840	4.19	0.87	0.054
S1	LP(1)	1.97230	S2–C5	$\sigma*$	0.02215	6.41	0.93	0.069
S1	LP(2)	1.81471	C5	LP*(1)	0.97108	60.19	0.08	0.079
S1	LP(2)	1.81471	C6–C7	$\sigma*$	0.02868	3.72	0.65	0.046
S2	LP(1)	1.97762	S1–C5	$\sigma*$	0.11755	4.36	0.85	0.056
S2	LP(1)	1.97762	N1–C5	$\sigma*$	0.06467	3.82	1.17	0.060
S2	LP(2)	1.82279	S1–C5	$\sigma*$	0.11755	16.29	0.34	0.067
S2	LP(2)	1.82279	N1–C5	$\sigma*$	0.06467	11.15	0.66	0.079
S2	LP(2)	1.82279	C6–H12	$\sigma*$	0.03148	3.74	0.61	0.044
S2	LP(3)	1.52985	C5	LP*(1)	0.97108	510.28	0.02	0.107
O1	LP(1)	1.96328	C8–C9	$\sigma*$	0.03488	6.60	1.08	0.075
O1	LP(1)	1.96328	C10–C11	$\sigma*$	0.05423	3.88	1.16	0.060
O1	LP(2)	1.74190	O2–C10	$\pi*$	0.27517	33.47	0.35	0.098
O1	LP(2)	1.74190	C8–C9	$\pi*$	0.42909	26.24	0.41	0.097
O2	LP(2)	1.82922	O1–C10	$\sigma*$	0.12872	38.15	0.56	0.132
O2	LP(2)	1.82922	C10–C11	$\sigma*$	0.05423	13.08	0.87	0.098
N1	LP(1)	1.60725	C5	LP*(1)	0.97108	185.64	0.09	0.135
N1	LP(1)	1.60725	C1–C2	$\sigma*$	0.01404	5.70	0.63	0.059
N1	LP(1)	1.60725	C3–C4	$\sigma*$	0.01228	5.29	0.64	0.058
O1–C10	$\sigma*$	0.12872	O1–C9	$\sigma*$	0.03147	20.65	0.04	0.087
O2–C10	$\pi*$	0.27517	C7–C11	$\pi*$	0.15842	100.07	0.02	0.076
C7–C11	$\pi*$	0.15842	C8–C9	$\pi*$	0.42909	49.00	0.04	0.073
C8–C9	$\pi*$	0.42909	C4–H10	$\sigma*$	0.00746	3.51	0.42	0.074
C8–C9	$\pi*$	0.42909	C8–C12	$\sigma*$	0.02242	7.13	0.80	0.142
C8–C9	$\pi*$	0.42909	C9–C15	$\sigma*$	0.02222	6.06	0.71	0.123
C8–C9	$\pi*$	0.42909	C10–C11	$\sigma*$	0.05423	5.07	0.54	0.095
C8–C9	$\pi*$	0.42909	C14–C15	$\sigma*$	0.02596	10.25	3.46	0.353
C8–C9	$\pi*$	0.42909	C14–C15	$\pi*$	0.37626	6.96	2.62	0.190
C8–C9	$\pi*$	0.42909	C15–H16	$\sigma*$	0.01243	8.92	3.30	0.326
C12–C13	$\pi*$	0.30508	C8–C9	$\pi*$	0.42909	97.80	0.05	0.101
C14–C15	$\pi*$	0.37626	C14–C15	$\sigma*$	0.02596	141.19	0.84	0.686
C14–C15	$\pi*$	0.37626	C15–H16	$\sigma*$	0.01243	407.02	0.67	1.060

[a] $E^{(2)}$, energy of hyper conjugative interactions.
[b] Energy difference between donor and acceptor i and j NBO orbitals.
[c] F_{ij} is the Fock matrix element between i and j NBO orbitals.

TABLE IV

Mulliken atomic charges of the title compound in gas phase and solution phase

Atom	In gas phase B3LYP 6-311++G(d,p)	In solution phase B3LYP/6-311++G(d,p)				
		Chloroform ($\varepsilon = 4.71$)	Ethanol ($\varepsilon = 24.55$)	Methanol ($\varepsilon = 32.61$)	DMSO ($\varepsilon = 46.82$)	Water ($\varepsilon = 78.36$)
Cl1	0.469	0.453	0.448	0.448	0.447	0.447
S1	−0.019	−0.034	−0.032	−0.032	−0.031	−0.031
S2	−0.561	−0.610	−0.639	−0.641	−0.644	−0.646
O1	−0.121	−0.132	−0.136	−0.137	−0.137	−0.137
O2	−0.259	−0.332	−0.360	−0.361	−0.363	−0.365
N1	0.481	0.491	0.493	0.494	0.494	0.494
C1	−0.366	−0.382	−0.390	−0.390	−0.391	−0.391
H1	0.143	0.152	0.155	0.155	0.156	0.156
C2	−0.335	−0.325	−0.318	−0.317	−0.317	−0.316
H2	0.147	0.146	0.145	0.145	0.145	0.145
C3	−0.188	−0.185	−0.189	−0.189	−0.190	−0.190
H3	0.144	0.152	0.154	0.154	0.155	0.155
C4	−0.392	−0.408	−0.413	−0.413	−0.414	−0.414
H4	0.171	0.188	0.194	0.194	0.195	0.195
C5	−0.481	−0.474	−0.466	−0.465	−0.464	−0.464
C6	0.042	−0.011	−0.044	−0.046	−0.049	−0.051
C7	0.939	0.989	1.023	1.026	1.028	1.031
C8	0.601	0.589	0.581	0.580	0.580	0.579
C9	−1.228	−1.224	−1.215	−1.215	−1.214	−1.213
H5	0.164	0.169	0.172	0.172	0.172	0.172
C10	0.151	0.204	0.226	0.227	0.229	0.230
H6	0.135	0.155	0.163	0.164	0.164	0.165
C11	−0.069	−0.101	−0.124	−0.126	−0.128	−0.131
C12	−0.507	−0.500	−0.493	−0.492	−0.491	−0.491
H7	0.152	0.146	0.143	0.142	0.142	0.142
C13	−0.846	−0.850	−0.861	−0.862	−0.863	−0.864
C14	0.572	0.564	0.563	0.563	0.563	0.563
H8	0.150	0.158	0.161	0.161	0.161	0.161
H9	0.161	0.151	0.146	0.146	0.145	0.145
C15	−0.529	−0.526	−0.517	−0.517	−0.516	−0.515
H10	0.127	0.137	0.142	0.143	0.143	0.143
H11	0.311	0.334	0.343	0.344	0.344	0.345
H12	0.115	0.126	0.137	0.138	0.140	0.141
H13	0.226	0.227	0.223	0.223	0.222	0.222
H14	0.080	0.109	0.118	0.118	0.119	0.119
H15	0.197	0.218	0.227	0.227	0.228	0.228
H16	0.223	0.237	0.240	0.240	0.240	0.240

The Mulliken analysis shows that carbon atoms attached with oxygen and nitrogen atoms are positive, however, the other carbon atoms have more negative charges. All hydrogen atoms have a positive charge and the oxygen and sulfur atoms are negatively charged. The carbon atoms attached with hydrogen atoms are negative, whereas C7, C8, C10, and C14 atoms are positively charged in all phases. The other carbon atoms have more negative atomic charges. The maximum positive atomic charge is obtained for C7 atom of carbonyl group when compared with all other atoms. C6 atom has only positive charge in gas phase. This behavior may be the result of C10=O2 double bond character and electronegativity of binding ring. Besides, in solution phase, the atomic charge values of the S1, S2, N1, O1, O2, C1, C4, C7, C10, C11, and C13 atoms are bigger than those in gas phase while their atomic charge values will increase with the increase in the polarity of the solvent except for methanol phase. Whereas, values of Cl1, C2, C5, C8, C9, C12, and C15 almost decrease with the increasing polarity of the solvent. These situation may be helpful to construct interesting metal complexes with different coordinate geometries [60].

3.5. Nonlinear optical effects

Nonlinear optics (NLO) is at the forefront of current research because of its importance in providing the key functions of frequency shifting, optical modulation, optical switching, optical logic, and optical memory for emerging technologies in areas such as telecommunications, signal processing, and optical interconnections [58, 61, 62].

The calculations of the total molecular dipole moment (μ_{tot}), linear polarizability (α_{tot}), and first-order hyperpolarizability (β_{tot}) from the Gaussian output have been explained in detail previously [63], and DFT has been used extensively as an effective method to investigate organic NLO materials [64]. The polar properties of the title compound were calculated at the B3LYP/6-311++G(d,p) level using the Gaussian 09W program package. The calculated values of μ_{tot}, α_{tot} and β_{tot} for the title compound are 7.470 D, 38.342 Å^3, and 4.917×10^{-30} esu which are greater than those of urea (the μ_{tot}, α_{tot} and β_{tot} of urea are 3.878 D, 5.042 Å^3 and 0.77×10^{-30} esu obtained by B3LYP/6-311++G(d,p) method). Theoretically, the first-order hyperpolarizability of the title compound is of 6.38 times magnitude of urea. When it is compared to the related compounds in the literature, the calculated value of β_{tot} of the title compound is bigger than that of 9-methoxy-2H-furo[3,2-g]chromen-2-one ($\beta_{\text{tot}} = 4.8988 \times 10^{-30}$ esu calculated with B3LYP/6-311++G(d,p) method) [65] and 3-(1-(((methoxycarbonyl)oxy)imino)ethyl)-2H-chromen-2-one ($\beta_{\text{tot}} = 1.403 \times 10^{-30}$ esu calculated with B3LYP/6-311++G(d,p) method) [66]. These results indicate that the title compound is a good candidate of NLO material.

3.6. MEP analysis

Electrostatic potential maps enable us to visualize the charge distributions of molecules and charge related properties of molecules. They also allow us to visualize the size, shape, and bond character of molecules. This knowledge of the charge distributions can be used to determine how molecules interact with one another. Also, the MEP is a useful feature to study reactivity given that an approaching electrophile will be initially attracted to negative regions (where the electron distribution effect is dominant). In the majority of the MEP, while areas of low potential, red, are characterized by an abundance of electrons, areas of high potential, blue, are characterized by a relative absence of electrons. Intermediary colors represent intermediary electrostatic potentials. Also the MEP is very useful in research of molecular structure with its physicochemical property relationship [67]. In this study, 3D plots of MEP of the title molecule are illustrated in Fig. 8.

As shown in Fig. 8, the electron density of the oxygen atoms is higher than the others. The negative regions in the molecule were found around the O2 atom. The negative $V(r)$ value is -0.102 a.u. for O2 atom which is the most negative region. Therefore, it can be predicted that

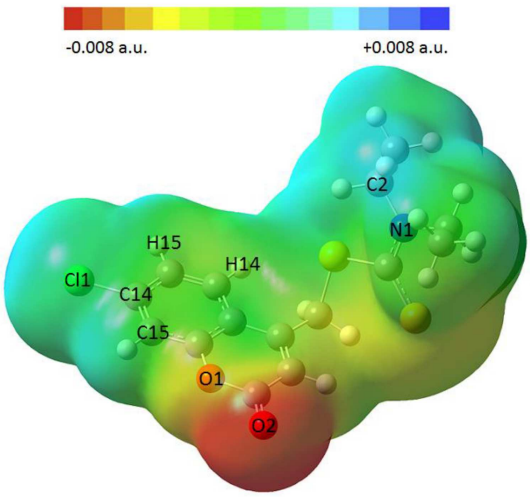

Fig. 8. The total electron density mapped with the electrostatic potential surface of the title compound.

an electrophile would preferably attack the title molecule at the O2 position. On the other hand, a maximum positive region is localized on the benzene ring with Cl atom in which values of hydrogens atoms (H14 and H15) are +0.065 a.u. indicating a possible site. Similarly, Cl1 and C15 values are +0.054 a.u. and +0.037 a.u., respectively. Additionally, the hydrogens in methile (near the C2 atom) have values ranging from +0.038 a.u. to +0.042 a.u. The MEP results of the title compound are in agreement with the literature [68].

According to these results, the MEP map indicated that the negative potential sites are on keto group and the positive potential sites are around the Cl and hydrogen atoms. These sites give information concerning the region from where the compound can have intermolecular interactions [58]. So, Fig. 8 confirms the existence of the intermolecular C–H...O interactions.

3.7. Frontier molecular orbital analysis

The frontier molecular orbitals play an important role in the electric and optical properties as well as in UV-vis spectra and chemical reactions [69]. Figure 9 shows the distributions and energy levels of the HOMO-1, HOMO, LUMO and LUMO+1 orbitals computed at the B3LYP/6-311++G(d,p) level for the title compound.

From the figure, HOMO-1 clouds are delocalised on the sulfur atoms and near the chromene ring while HOMO clouds are delocalised on the sulfur atoms. For the LUMO, the electrons are mainly delocalised on the 7-chloro-2-oxo-2H-chromen ring. The value of the energy separation between the HOMO and LUMO is 3.9149 eV. This large HOMO-LUMO gap could give us information about high excitation energies for many of excited states, stability, and a high chemical hardness for the title compound [70].

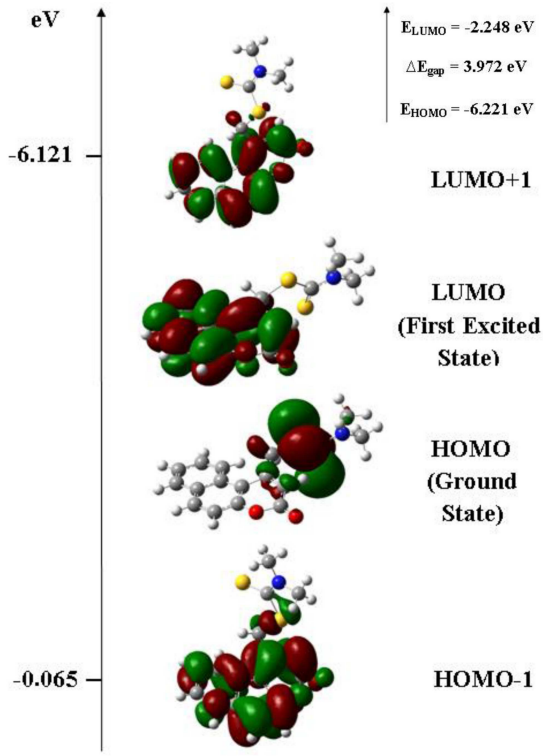

Fig. 9. Molecular orbital surfaces and energy levels given in parentheses for the HOMO-1, HOMO, LUMO, and LUMO+1 of the title compound computed at B3LYP/6-311++G(d,p) level.

3.8. Thermodynamic properties

Vibrational analysis and statistical thermodynamics, the standard thermodynamic functions entropy (S_m^0), heat capacity ($C_{p,m}^0$), and enthalpy (H_m^0) were obtained using basis of B3LYP/6-311++G(d,p) moving the energy situation like frontier molecular orbital analysis and are listed in Table V. The scale factor for frequencies is 0.96 which is used for an accurate prediction in determining the thermodynamic functions. The table shows that the S_m^0, $C_{p,m}^0$, and H_m^0 increase at any temperature from 200 to 600 K, because the intensities of the molecular vibration increase with the increase of temperature.

The correlations between these thermodynamic properties and temperatures T are shown in Fig. 10. The correlation equations are as follows:

$$C_{p,m}^0 = 1.99445 + 0.30903T - 1.50319 \times 10^{-4}T^2,$$
$$(R^2 = 0.99989)$$
$$S_m^0 = 69.3273 + 0.33024T - 8.83606 \times 10^{-5}T^2,$$
$$(R^2 = 1)$$
$$H_m^0 = -1.98092 + 0.02608T - 9.50872 \times 10^{-5}T^2,$$
$$(R^2 = 0.99995)$$

These equations will be helpful for the further studies of the title compound.

TABLE V

Thermodynamic properties at different temperatures at B3LYP/6-311++G(d,p) level

T [K]	H_m [kcal mol^{-1}]	$C_{p,m}$ [cal mol^{-1} K^{-1}]	S_m [cal mol^{-1} K^{-1}]
200	7.2	58.2	131.8
250	10.5	69.6	146.4
298.15	14.2	80.5	160.0
300	14.3	80.9	160.5
350	18.7	91.7	174.1
400	23.7	101.7	187.3
450	29.1	110.9	200.0
500	34.9	119.1	212.3
550	41.2	126.5	224.2
600	47.8	133.1	235.7

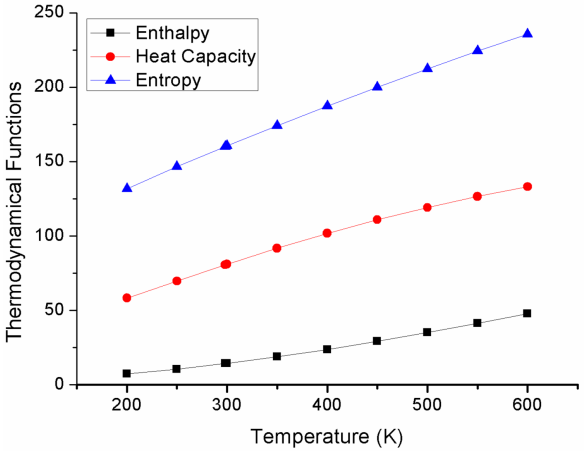

Fig. 10. Correlation graphics of thermodynamic properties and temperatures.

4. Conclusions

In this study, we tested the different HF, B3LYP, and B3PW91 levels of theory using the 6-311++G(d,p) basis set. The computed geometric parameters and vibrational frequencies of the title compound have been compared with experimental data. This study demonstrates that DFT calculations are a good approach for understanding the molecular structure and vibrational spectra of the title molecule, in which the experimental and theoretical results support each other.

The MEP map shows that the negative potential sites are on electronegative atoms and that the positive potential sites are around the hydrogen atoms. These sites give information about the region from where the compound can have intramolecular interactions. The value of the energy separation between the HOMO and LUMO is very large and this energy gap gives significant informations about the title compound. The NBO analysis revealed that π^*-electrons with the greater energy contributions from C20–C21 $\rightarrow$ σ^*(C21–H16) (407.02 kcal/mol) and σ^*(C20–C21)(141.19 kcal/mol). Also, molecule involves

electron density transfer from lone pair of S3 to antibonding LP*(1)(C11) atom to achieve enormous stabilization (up to 510.28 kcal/mol). Besides, charge distribution of title compound is performed comparatively by using of the natural population analysis in several solvents and gas phase. The correlations between the statistical thermodynamic properties (enthalpy, entropy, heat capacity) and temperatures are also obtained. We hope that our paper will be helpful to analyze and synthesize new materials.

References

[1] P. Laurin, D. Ferroud, M. Klich, C. Dupuis-Hamelin, P. Mauvais, P. Lassaigne, A. Bonnefoy, B. Musicki, *Bioorg. Med. Chem. Lett.* **9**, 2079 (1999).

[2] P.N. Sharma, A. Shoeb, R.S. Kapil, S.P. Popli, *Indian J. Chem. B* **19**, 938 (1980).

[3] A.C.T. North, D.C. Philips, F.S. Mathews, *Acta Crystallogr. A* **24**, 351 (1968).

[4] K.C. Fylaktakidou, D.J. Hadjipavlou-Litina, K.E. Litinas, D.N. Nicolaides, *Curr. Pharm. Des.* **10**, 3813 (2004).

[5] M.K. Aliaa, M.K. Manal, K. Abd El-all Eman, A.H. Elshemy Heba, *Int. J. Pharm. Res. Develop.* **4**, 310 (2012).

[6] M. Traykova, I. Kostova, *Int. J. Pharm.* **1**, 29 (2005).

[7] R.K. Nimesh, D.H. Dhaval, T.M. Prashant, K.P. Saurabh, *Med. Chem. Res.* **20**, 854 (2011).

[8] Z.M. Nofal, M. El-Zahar, S. Abd El-Karim, *Molecules* **5**, 99 (2000).

[9] G. Henriette, L. Lorraine, H. Bettina, D. Clemence, D. Kelly, K. Irenej, *Mol. Cancer Ther.* **3**, 1375 (2004).

[10] C. Kwangwoo, P. Song-Kyu, K.H. Mook, C. Yongseok, K. Myung-Hwa, P. Chun-Ho, J. Bo-Young, C.T. Gyu, C. Hyun-Moo, L. Hee-Yoon, H.S. Hee, K.M. Sook, N. Ky-Youb, H. Gyoonhee, *Bioorg. Med. Chem.* **16**, 530 (2008).

[11] I. Manolov, N.D. Danchev, *Eur. J. Med. Chem. Chim. Ther.* **30**, 531 (1995).

[12] J. Nareshkumar, X. Jiayi, M.K. Ramesh, D. Fuyong, J.Z. Guo, P. Emmanuel, *J. Med. Chem.* **52**, 7544 (2009).

[13] A.A. Emmanuel-Giota, K.C. Fylaktakidou, D.J. Hadjipavlou-Latina, K.E. Litinas, D.N. Nicolaides, *J. Heterocycl. Chem.* **38**, 717 (2001).

[14] M. Cacic, M. Trkovnik, F. Cacic, E. Has-Schon, *Molecules* **11**, 134 (2006).

[15] M.A. Bhat, N. Siddiqui, S.A. Khan, *Acta Pol. Pharm.* **65**, 235 (2008).

[16] G. Jones, W.R. Jackson, C. Choi, W.R. Bergmark, *J. Phys. Chem.* **89**, 294 (1985).

[17] S.R. Trenor, A.R. Shultz, B.J. Love, T.E. Long, *Chem. Rev.* **104**, 3059 (2004).

[18] T.T. Hung, Y.J. Lu, W.Y. Liao, C.L. Huang, *IEEE Trans. Magn.* **43**, 867 (2007).

[19] J.B. Wang, X.H. Qian, J.N. Cui, *J. Org. Chem.* **71**, 4308 (2006).

[20] K.M. Kumar, D. Kour, K. Kapoor, N.M. Mahabaleshwaraiah, O. Kotresh, V.K. Gupta, R. Kant, *Acta Cryst. Sect. E Struct. Rep. Online* **68**, o878 (2012).

[21] M. Zahradnik, *The Production and Applications of Fluorescent Brightening Agent*, Wiley, Chichester, UK 1992.

[22] R.O. Kennedy, R.D. Thornes, *Coumarins: Biology, Applications and Mode of Action*, Wiley, Chichester, UK 1997.

[23] Y. Zhang, Z. Guo, X.Z. You, *J. Am. Chem. Soc.* **123**, 9378 (2001).

[24] F. De Proft, P. Geerlings, *Chem. Rev.* **101**, 1451 (2001).

[25] B.G. Johnson, P.M.W. Gill, J.A. Pople, *J. Chem. Phys.* **98**, 5612 (1993).

[26] N. Oliphant, R.J. Bartlett, *J. Chem. Phys.* **100**, 6550 (1994).

[27] A.A. Agar, H. Tanak, M. Yavuz, *Mol. Phys.* **108**, 1759 (2010).

[28] T.G. Meenakshi, J. Shylajakumari, H.C. Devarajegowda, K. Mahesh Kumar, O. Kotresh, *Acta Crystallogr. Sect. E Struct. Rep. Online* **69**, 1431 (2013).

[29] M.J. Frisch, G.W. Trucks, H.B. Schlegel, G.E. Suzerain, M.A. Robb, J.R. Cheeseman Jr., J.A. Montgomery, T. Vreven, K.N. Kudin, J.C. Burant, J.M. Millam, S.S. Iyengar, J. Tomasi, V. Barone, B. Mennucci, M. Cossi, G. Scalmani, N. Rega, G.A. Petersson, H. Nakatsuji, M. Hada, M. Ehara, K. Toyota, R. Fukuda, J. Hasegawa, M. Ishida, T. Nakajima, Y. Honda, O. Kitao, H. Nakai, M. Klene, X. Li, J.E. Knox, H.P. Hratchian, J.B. Cross, V. Bakken, C. Adamo, J. Jaramillo, R. Gomperts, R.E. Stratmann, O. Yazyev, A.J. Austin, R. Cammi, C. Pomelli, J.W. Ochterski, P.Y. Ayala, K. Morokuma, G.A. Voth, P. Salvador, J.J. Dannenberg, V.G. Zakrzewski, S. Dapprich, A.D. Daniels, M.C. Strain, O. Farkas, D.K. Malick, A.D. Rabuck, K. Raghavachari, J.B. Foresman, J.V. Ortiz, Q. Cui, A.G. Baboul, S. Clifford, J. Cioslowski, B. Stefanov, G. Liu, A. Liashenko, P. Piskorz, I. Komaromi, R.L. Martin, D.J. Fox, T. Keith, M.A. Al-Laham, C.Y. Peng, A. Nanayakkara, M. Challacombe, P.M.W. Gill, B. Johnson, W. Chen, M.W. Wong, C. Gonzalez, J.A. Pople, Gaussian 09 (now Gaussian 16), Gaussian Inc., Wallingford (CT) 2016.

[30] R. Dennington, T. Keith, J. Millam, Semichem Inc., Shawnee Mission KS, GaussView, Version 5, 2009.

[31] G.A. Zhurko, ChemCraft, version 1.6 (build 304), 2009.

[32] H. Tanak, *J. Mol. Struct. (Theochem)* **950**, 5 (2010).

[33] M. Evecen, H. Tanak, N. Dege, M. Kara, O.E. Dogan, E. Ağar, *Mol. Cryst. Liq. Cryst.* **648**, 183 (2017).

[34] P.D. Babu, S. Periandy, S. Mohan, S. Ramalingam, B.G. Jayaprakash, *Spectrochim. Acta A Mol. Biomol. Spectrosc.* **78**, 168 (2011).

[35] N. Sundaraganesan, S. Ilakiamani, H. Saleem, P.M. Wojciechowski, D. Michalska, *Spectrochim. Acta A Mol. Biomol. Spectrosc.* **61**, 2995 (2005).

[36] V. Krishnakumar, R. John Xavier, *Indian J. Pure. Appl. Phys.* **41**, 597 (2003).

[37] H. Tanak, A.A. Agar, O. Büyükgüngör, *Spectrochim. Acta Part A Mol. Biomol. Spectrosc.* **87**, 15 (2012).

[38] R.N. Singh, S.C. Prasad, *Spectrochim. Acta A* **34**, 39 (1974).

[39] R.M. Silverstein, G. Clayton Bassler, T.C. Morril, *Spectroscopic Identification of Organic Compounds*, Wiley, New York 1991.

[40] A. Altun, K. Gölcük, M. Kumru, *J. Mol. Struct. (Theochem)* **625**, 17 (2003).

[41] J.R. Durig, M.M. Bergana, H.V. Phan, *J. Raman Spectrosc.* **22**, 141 (1991).

[42] G. Litivinov, in: *Proc. XIII Int. Conf. on Raman Spectroscopy, Würzburg (Germany)*, 1992.

[43] M. Govindarajan, K. Ganasan, S. Periandy, S. Mohan, *Spectrochim. Acta A Mol. Biomol. Spectrosc.* **76**, 12 (2010).

[44] R.M. Silverstein, G.C. Bassler, C. Morrill, *Spectrometric Identification of Organic Compounds*, Wiley, New York 1981.

[45] T. Karakurt, M. Dinçer, A. Çukurovalı, İ. Yılmaz, *J. Mol. Struct.* **991**, 186 (2011).

[46] M.M.J. Tecklenburg, D.J. Kosnak, A. Bhatnagar, D.K. Mohanty, *J. Raman Spectrosc.* **28**, 755 (1997).

[47] J. Pająk, M. Rospenk, R. Ramaekers, G. Maes, T. Głowiak, L. Sobczyk, *Chem. Phys.* **278**, 89 (2002).

[48] M. Arivazhagan, V. Krishnakumar, R. John Xavier, V. Ilango, K. Balachandran, *Spectrochim. Acta A Mol. Biomol. Spectrosc.* **72**, 941 (2009).

[49] G. Varsanyi, *Vibrational Spectra of Benzene Derivatives*, Academic Press, New York 1969.

[50] R.M. Silverstein, F.X. Webstor, *Spectrometric Identification of Organic Compounds*, 6th ed., Wiley, New York 1998.

[51] N.B. Colthup, L.H. Daly, S.E. Wiberly, *Introduction to Infrared and Raman Spectroscopy*, 3rd ed., Academic Press, Boston (MA) 1990.

[52] G. Socrates, *Infrared Characteristic Group Frequencies*, Wiley, New York 1980.

[53] C. James, A. Amal Raj, R. Reghunathan, I. Hubert Joe, V.S. Jayakumar, *J. Raman Spectrosc.* **37**, 1381 (2006).

[54] J.N. Liu, Z.R. Chen, S.F. Yuan, *J. Zhejiang Univ. Sci. B* **6**, 584 (2005).

[55] S. Muthu, M. Prasath, *Spectrochim. Acta A Mol. Biomol. Spectrosc.* **115**, 789 (2013).

[56] D.W. Schwenke, D.G. Truhlar, *J. Chem. Phys.* **82**, 2418 (1985).

[57] M. Gutowski, G. Chal, *J. Chem. Phys.* **98**, 5540 (1993).

[58] H. Tanak, A.A. Agar, O. Büyükgüngör, *Spectrochim. Acta A Mol. Biomol. Spectrosc.* **118**, 672 (2014).

[59] I.G. Csizmadia, *Theory and Practice of MO Calculations on Organic Molecules*, Elsevier, Amsterdam 1976.

[60] F.F. Jian, P.S. Zhao, Z.S. Bai, L. Zhang, *Struct. Chem.* **16**, 635 (2005).

[61] V.M. Geskin, C. Lambert, J.L. Bredas, *J. Am. Chem. Soc.* **125**, 15651 (2003).

[62] M. Nakano, H. Fujita, M. Takahata, K. Yamaguchi, *J. Am. Chem. Soc.* **124**, 9648 (2002).

[63] K.S. Thanthiriwatte, K.M. Nalin de Silva, *J. Mol. Struct. (Theochem)* **617**, 169 (2002).

[64] H. Tanak, K. Pawlus, M.K. Marchewka, A. Pietraszko, *Spectrochim. Acta A Mol. Biomol. Spectrosc.* **118**, 82 (2014).

[65] N. Swarnalatha, S. Gunasekaran, S. Muthu, M. Nagarajan, *Spectrochim. Acta A Mol. Biomol. Spectrosc.* **137**, 721 (2015).

[66] K.G. Krishnan, R. Sivakumar, V. Thanikachalam, H. Saleem, *Spectrochim. Acta A Mol. Biomol. Spectrosc.* **144**, 29 (2015).

[67] E. Inkaya, M. Dincer, E. Sahan, E. Korkusuz, I. Yıldırım, O. Buyukgungor, *J. Mol. Struct.* **1039**, 179 (2013).

[68] H. Tanak, M. Toy, *J. Mol. Struct.* **1068**, 189 (2014).

[69] I. Fleming, *Frontier Orbitals and Organic Chemical Reactions*, Wiley, London 1976.

[70] N. Günay, Ö. Tamer, D. Kuzalic, D. Avcı, Y. Atalay, *Acta Phys. Pol. A* **127**, 701 (2015).